PCCP

Dynamic Article Links

View Online

Cite this: DOI: 10.1039/c0cp02231d

www.rsc.org/pccp

PAPER

Electronic coherences and vibrational wave-packets in single molecules studied with femtosecond phase-controlled spectroscopy

Richard Hildner,*[a] Daan Brinks,[a] Fernando D. Stefani†[a] and Niek F. van Hulst*[ab]

Received 21st October 2010, Accepted 4th January 2011
DOI: 10.1039/c0cp02231d

Employing femtosecond pulse-shaping techniques we investigate ultrafast, coherent and incoherent dynamics in single molecules at room temperature. In first experiments single molecules are excited into their purely electronic 0–0 transition by phase-locked double-pulse sequences with pulse durations of 75 fs and 20 nm spectral band width. Their femtosecond kinetics can then be understood in terms of a 2-level system and modelled with the optical Bloch equations. We find that we observe the coherence decay in single molecules, and the purely electronic dephasing times can be retrieved directly in the time domain. In addition, the Rabi-frequencies and thus the transition dipole moments of single molecules are determined from these data. Upon excitation of single molecules into a vibrational level of the electronically excited state also incoherent intra-molecular vibrational relaxation is recorded. Increasing the spectral band width of the excitation pulses to up to 120 nm (resulting in a transform-limited pulse width of 15 fs) coherent superpositions of excited state vibrational modes, *i.e.* vibrational wave packets, are excited. The wave-packet oscillations in the excited state potential energy surface are followed in time by a phase-controlled pump–probe scheme, which permits to record wave packet interference, and to determine the energies of vibrational modes and their coupling strengths to the electronic transition.

Introduction

Since their first demonstration[1] single-molecule techniques have developed into a versatile tool and have been employed to study a wide variety of processes and systems, such as protein interactions,[2] cellular processes,[3] the behaviour of supercooled liquids,[4] and the electronic structure of synthetic[5] and natural[6] light-harvesting systems. Single molecules have also been used as nanoprobes for local fields and density of states near plasmonic structures[7] and have even been demonstrated to show transistor-like behaviour for light.[8] Despite this remarkable development in the last two decades, many relevant processes, as *e.g.* excitation energy transfer in molecular assemblies, were not directly accessible on the single-molecule level so far. These processes typically occur on (sub-)picosecond time scales at room temperature,[9] whereas the time-resolution of single-molecule techniques was limited to some tens of picoseconds, as achieved with time-correlated single-photon counting. Moreover, evidence is growing that quantum coherences play a significant role in the initial ultrafast steps of excitation energy transfer in photosynthetic assemblies,[10] conjugated polymers,[11] and dendritic systems[12] at room temperature. Therefore it would be highly interesting to investigate such typically highly heterogeneous molecular assemblies with an ultrafast single-molecule technique that allows both coherent and incoherent processes to be addressed.

Previously, van Dijk *et al.* achieved a time-resolution of about 100 fs in single-molecule experiments with a fluorescence-detected pump–probe scheme and investigated incoherent excited state vibrational relaxation in individual molecules and coupled molecular systems at room temperature.[13,14] Very recently, we extended the time-resolution further to *ca.* 10 fs by employing pulse-shaping techniques. We demonstrated that vibrational[15] and electronic coherences[16] in single molecules can be resolved and even manipulated at room temperature despite pure electronic dephasing times of about 50 fs and depending on the detection of incoherent fluorescence. In these experiments we excited single molecules with ultrashort pulses (15–75 fs) and created coherent superposition states. The time evolution and decay of the coherent superposition state was then interrogated with a second delayed pulse. The key in these pulse-shaping experiments is the full control over the relative phase between both pulses, since the second pulse can then probe the phase memory in the wavefunctions of the coherent

---

[a] *ICFO, Institut de Ciencies Fotoniques, Mediterranean Technology Park, 08860 Castelldefels, Barcelona, Spain. E-mail: richard.hildner@icfo.es, niek.vanHulst@icfo.es; Fax: +34 935534000*
[b] *ICREA, Institucio Catalana de Recerca i Estudis Avancats, 08015 Barcelona, Spain*

† Present address: Departamento de Física & Instituto de Física de Buenos Aires (IFIBA, CONICET), Universidad de Buenos Aires, Pab. I Ciudad Universitaria, 1428 Buenos Aires, Argentina.

superposition state created by the first pulse. After interaction of the molecule with such pulse sequences the excited state population probability, and thus the incoherent fluorescence signal, becomes a function of both inter-pulse delay time and phase difference, and can be related to molecular properties.

Here we discuss different femtosecond excitation schemes on single molecules and show the various aspects that can be addressed with these techniques, such as the electronic coherence decay and vibrational wave-packet interference. We further demonstrate that many photophysical parameters can be retrieved from these single-molecule data, *e.g.* transition dipole moments, pure electronic dephasing times, incoherent vibrational relaxation times, and vibrational energies.

Experimental

We employed two excitation schemes to investigate individual molecules on sub-100 fs time scales (Fig. 1, box 1). First, to excite only the purely electronic transition, we used pulses with a spectral band width of about 20 nm ($\sim 500\ \mathrm{cm}^{-1}$). This is less than the line widths of single-molecule emission spectra at room temperature and is thus a reasonable compromise between a relatively narrow laser band width and a sub-100 fs transform-limited pulse duration. These pulses had centre wavelengths between 622 and 640 nm and were produced by an optical parametric oscillator (OPO, Automatic PP, APE, pumped by a Titanium:Sapphire-system, Mira, Coherent). The output of the OPO was sent through a pulse picker (PulseSelect, APE) to reduce the repetition rate from 76 MHz to effectively 500 kHz (bunches of pulses with a repetition rate of 25 kHz, repetition rate within bunches: 4 MHz). This matches the input of an acousto-optic programmable dispersive filter (AOPDF, Dazzler, Fastlite, see Fig. 1, box 2), that was used both for dispersion compensation to provide transform limited pulses with 75 fs duration at the sample plane, as well as for pulse shaping to generate pulse sequences with a well-defined delay time Δt and relative phase ϕ.

Second, for broadband coherent excitation of a manifold of vibrational levels in the electronically excited state, the output of a Titanium:Sapphire-laser (Octavius 85M, Menlo Systems) with a spectral band width of 120 nm ($2650\ \mathrm{cm}^{-1}$) was used, which covers nearly the entire absorption spectrum of a single molecule. The central wavelength was 676 nm and the repetition rate 85 MHz. Since the AOPDF can not handle such large spectral band widths, we employed instead a 4f-pulse shaper based on a spatial light modulator for dispersion control and shaping (adapted from MIIPS-Box, Biophotonics Solutions Inc.). The shaper is designed in a double-pass configuration (Fig. 1, box 3),[17] where a mirror at the end of the beam path reflects the light back through the shaper. This avoids the introduction of spatio-temporal coupling in the shaper[18] and allows larger phase distortions to be compensated. The pulses were compressed to their transform limit of 15 fs at the sample plane.

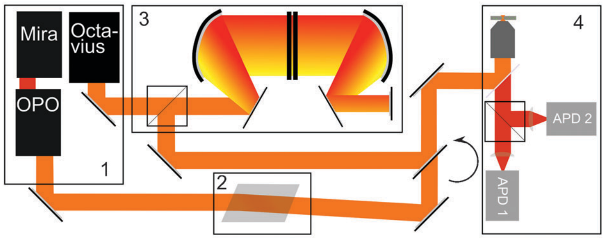

Fig. 1 Experimental setup. 1: Femtosecond laser sources; 2: acousto-optic programmable dispersive filter for pulse shaping of a "narrowband" (20 nm band width) laser system; 3: 4f-pulse shaper based on a spatial light modulator for pulse shaping of a broadband (120 nm band width) laser system; 4: confocal microscope. See text for details.

The shaped pulses were then spatially filtered in a lens-pinhole-lens combination, directed into a confocal microscope (Fig. 1, box 4), and focussed onto the single-molecule sample with a 1.3 NA objective (Fluar, Zeiss). The fluorescence was separated from the excitation light with suitable dichroic beam splitters and long pass filters, and split on two sensitive photodiodes (APD, Perkin Elmer) by a polarising beam splitter. The excitation power was simultaneously recorded with a photodiode at the sample position. A measurement consisted of scanning the sample with a piezo stage (Mad City Labs) to image the fluorescence intensity as a function of position, bringing single molecules consecutively into the focus of the excitation beam, and recording the fluorescence signal of each molecule as a function of the pulse shape until photobleaching.

The molecules used for our investigations were chosen to spectrally match the excitation conditions while featuring good photostability and high fluorescence quantum yields: in the experiments employing 75 fs pulses and the AOPDF for pulse-shaping, the 20 nm spectral band width could only be achieved for centre wavelengths between 622 and 640 nm. Here we used terrylenediimide (TDI) that has an absorption maximum at *ca.* 640 nm in bulk solution[19] and is thus near-resonantly excited into its purely electronic transition.

For the experiments using 15 fs pulses and the SLM for pulse shaping the spectrum was centred at 676 nm, which was the spectrum with the lowest central wavelength carrying sufficient intensity across the entire 120 nm band to allow for accurate phase compensation and pulse shaping. Here we used a homologue of terrylene, dinaphtoquaterrylenebis-(dicarboximide) (DNQDI). The absorption spectrum of DNQDI extends from *ca.* 550 to 750 nm with a maximum at 700 nm (in toluene solution)[20] and nicely overlaps with the broadband laser spectrum.

All samples were prepared by dissolving the respective molecules together with poly(methyl-metacrylate), PMMA, in toluene and spincoating this solution onto microscope cover slips. The concentrations of both TDI and DNQDI were about 10^{-9} M resulting in less than one molecule per $\mu\mathrm{m}^2$ in 40 nm thick layers.

Results and discussion

a) 2-level system

In the first set of experiments we excited single TDI-molecules by phase-locked double-pulse sequences into (the high-energy tail of) their purely electronic transition (transition $|1\rangle \leftrightarrow |2\rangle$ in Fig. 2a, pulse width 75 fs, see above). In Fig. 2b and c (black

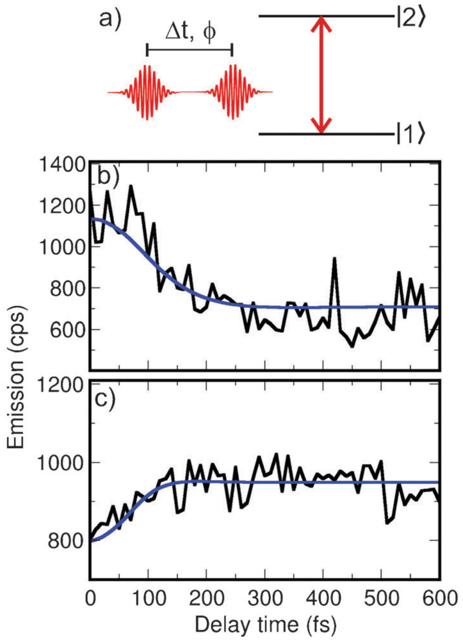

Fig. 2 Ultrafast double-pulse excitation of a 2-level system at room temperature. (a) A single molecule, described as a 2-level system with the electronic ground (|1⟩) and excited state (|2⟩), is resonantly excited by a phase-locked double-pulse sequence. (b) and (c) Black lines: Fluorescence as a function of the delay time Δt between the pulses for two single molecules (ϕ = 0 rad; cps: counts per second). Blue lines: Numerical simulations based on the optical Bloch equations for a 2-level system yielding: (b) $\omega_{R,0}$ = 0.03 fs^{-1}, γ_2* = 0.013 fs^{-1}, δ = 30 cm^{-1}, $\mu_{12,\text{eff}}$ = 3.3 D; (c) $\omega_{R,0}$ = 0.065 fs^{-1}, γ_2* = 0.02 fs^{-1}, δ = 0 cm^{-1}, $\mu_{12,\text{eff}}$ = 7.2 D.

lines) we show the emission signals of two different TDI-molecules as a function of the delay time Δt between the pulses. The relative phase was fixed at ϕ = 0 rad and the time-averaged excitation power was kept constant throughout the acquisition of each trace. The delay traces recorded from these molecules are clearly different and feature decaying (Fig. 2b) and rising (Fig. 2c) fluorescence signals, respectively, with time constants of several tens of femtoseconds in both cases. At long delay times the measured count rates are 700 cps for the trace in Fig. 2b (cps: counts per second, average between Δt = 550 and 600 fs) and 920 cps for the curve in Fig. 2c.

Since the excitation intensity was constant during measurement of each trace, the observed emission variations at short delays must come from the intrinsic ultrafast dynamics of single TDI-molecules. Given the excited state lifetime of 3.5 ns for TDI in PMMA and the fluorescence quantum yield of unity,[21] excited state population relaxation (intersystem crossing, internal conversion, or spontaneous emission) is negligible on time scales of the maximum delays used in our experiments (600 fs). Hence, the variations in the emission signals displayed in Fig. 2b and c are ascribed to the coherence decay in single molecules, *i.e.* the decay of the coherent superposition between the electronic ground and excited state wavefunctions, as we have shown recently.[16] The coherent superposition state is created by the interaction with the external laser field. Due to scattering with host vibrations (pure electronic dephasing processes),[22] however, these coherences decay on ultrafast time scales of typically several 10 fs for molecules embedded in disordered matrices at room temperature. We are able to record the coherence decay (or optical free induction decay) with our double-pulse excitation scheme, because the precise control of the relative phase between the pulses allows us to probe the (persistence or loss of) phase memory between the electronic wavefunctions induced by the first pulse.

The differences in the shapes of the delay traces in Fig. 2 result from varying interaction strengths between the molecular transition dipole moments and the laser pulses, *i.e.* varying Rabi-frequencies:[16] For small Rabi-frequencies we generally observe a decaying fluorescence signal as a function of the delay time (Fig. 2b). In this situation only absorption processes take place, but the transfer of population probability to the excited state becomes less efficient with increasing Δt due to pure electronic dephasing processes. At higher Rabi-frequencies also stimulated emission during interaction with the laser pulses occurs, *i.e.* population probability is pumped to the excited state and immediately dumped back to the ground state (Rabi-oscillation). For longer delays pure dephasing processes render mainly the dumping process to the ground state less efficient, leading to an increasing excited state population and thus rising emission signal (Fig. 2c). These differences in the interaction strengths between the molecules and the laser fields are also manifested in the higher count rate of 920 cps (at Δt = 600 fs) observed for the curve in Fig. 2c as compared to 700 cps for the trace in Fig. 2b.

To extract photophysical information from these data we performed simulations based on the density matrix ρ for a 2-level system in the rotating-wave approximation.[23] The density matrix is then a set of four coupled differential equations with four adjustable parameters: the excited state lifetime T_1, the dephasing rate $\gamma_2 = (2\cdot T_1)^{-1} + \gamma_2{}^*$ (γ_2*: pure electronic dephasing rate), the detuning δ between the transition frequency of the 2-level system and the central laser frequency, as well as the Rabi-frequency ω_R. However, for our experimental situation the equations can be simplified and incoherent population decay of the excited state with T_1 = 3.5 ns (relaxation of the diagonal elements of ρ) can be neglected, because we are interested only in the ultrafast dynamics up to 600 fs. Then γ_2 reduces to the pure dephasing rate γ_2* that describes the loss of phase memory between the electronic wavefunctions (relaxation of the off-diagonal elements of ρ). The detuning δ accounts for the slightly off-resonant excitation of the electronic transition as well as for static disorder that gives rise to a distribution of transition frequencies of individual TDI-molecules.[24,25] The Rabi-frequency is time-dependent in our pulsed experiment and given by

$$\omega_R(t) = \frac{\vec{\mu}_{12}\cdot\vec{E}(t)}{\hbar} = \frac{\vec{\mu}_{12}\cdot\vec{E}_0}{\hbar}\cdot f(t) = \omega_{R,0}\cdot f(t)$$

Here, $\vec{\mu}_{12}$ denotes the transition dipole moment between the electronic ground and excited state, and the exciting laser field $\vec{E}(t)$ is decomposed into the peak amplitude $\vec{E}_0$ and the time-dependent envelope function $f(t) = \exp\left(-\frac{t^2}{2\tau_p^2}\right) + \exp\left(-\frac{(t-\Delta t)^2}{2\tau_p^2}\right)$ (τ_p: pulse width). The time-independent maximum Rabi-frequency $\omega_{R,0} = \frac{\vec{\mu}_{12}\cdot\vec{E}_0}{\hbar}$ is varied in the simulations to account for different excitation intensities, random orientations of $\vec{\mu}_{12}$, as well as a distribution of the magnitude of $\vec{\mu}_{12}$.

The elements of the density matrix were calculated as a function of the delay time after the double-pulse sequence interacted with the two-level system. Here, we are particularly interested in the excited state population probability as a function of Δt, $\rho_{22}(\Delta t)$, because it is directly proportional to the emission signals recorded from single molecules. The calculated $\rho_{22}(\Delta t)$-curves were fitted to the delay traces by varying the free parameters ($\omega_{R,0}$, γ_2*, δ) and minimising the residuals between data and simulations. Further details can be found in ref. 16.

The simulated curves reproduce the data very well (Fig. 2b and c blue lines). The resulting histograms of the retrieved fit parameters are displayed in Fig. 3 for a total of 53 molecules, for which we could measure a delay trace at least twice. The detuning δ was found to be up to 80 cm^{-1} (Fig. 3a). These values are rather small given that the electronic transition energies of individual TDI-molecules are expected to be spread out under a broad inhomogeneous distribution of 305 cm^{-1} width (FWHM).[25] However, in our single-molecule experiment the distribution of δ is biased towards small values, because we selected only the brightest molecules that tend to have the smallest detuning, or in other words, the best overlap between the laser line and the particular single-molecule absorption spectrum.

The pure dephasing rates are distributed between 0.01 and 0.04 fs^{-1} (T_2* ~ 25–110 fs) with a maximum at 0.016 fs^{-1} (60 fs, see Fig. 3b), which is consistent with frequency-domain data on single terrylenes[25] as well as with photon-echo ensemble measurements on dye-molecules, all embedded in PMMA at room temperature.[26] The broad distribution of γ_2* is a consequence of the varying surroundings from molecule to molecule in the highly disordered, amorphous PMMA-film.

The maximum Rabi-frequencies $\omega_{R,0}$ range from 0.01 to 0.2 fs^{-1} (Fig. 3c). An important aspect of this data is that the distribution of transition dipole moments, or equivalently absorption cross-sections, of single chromophores is directly accessible, because the peak amplitude of the electric field E_0 can be calculated from the known repetition rate, pulse width, and time-averaged excitation intensity at the sample that was measured simultaneously with the delay traces. However, the TDI-molecules are randomly oriented in the PMMA-film, and only the projection of $\vec{\mu}_{12}$ onto the focal plane can be determined. For this "effective" transition dipole moment $\mu_{12,\text{eff}}$ we found a broad distribution between 1.1 and 22 D with a maximum at *ca.* 4 D (Fig. 3d). Since our model includes only the purely electronic transition, the coupling of vibrational modes to the electronic transition in a real molecule has to be accounted for by weighting $\mu_{12,\text{eff}}$ with the Debye–Waller factor α.[27] From the ensemble absorption spectrum we estimated $\alpha \approx 0.55$, which results in an effective transition dipole moment $\mu_{\text{eff}} = \mu_{12,\text{eff}}/\sqrt{\alpha}$ between 1.5 and 30 D (not shown) in agreement with bulk data on TDI.[28] Importantly, these μ_{eff}-values represent lower boundaries for the absolute transition dipole moments of individual TDI-molecules irrespective of their orientations. Our technique might be combined *e.g.* with defocused widefield imaging methods to get the full 3-dimensional orientation of the transition dipole moments,[29] and consequently absolute values may be determined.

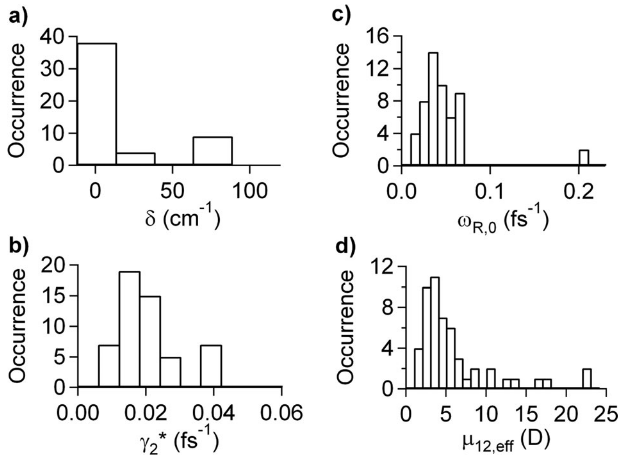

Fig. 3 Histograms of the fit parameters from simulations based on the 2-level system: (a) detuning δ, (b) pure dephasing rate γ_2*, (c) maximum Rabi-frequency $\omega_{R,0}$, and (d) effective transition dipole moment $\mu_{12,\text{eff}}$.

Recently, other groups also reported absolute cross-section measurements on single molecules at room temperature. Celebrano *et al.*[30] employed a differential transmission technique, while Gaiduk *et al.*[31] exploited photothermal contrast upon intense illumination, to determine the absorption cross-sections of individual molecules. The approach of Kastrup and Hell[32] is based on stimulated emission depletion (STED) and measures in fact the stimulated emission cross-section for the STED-transition, *i.e.* the transition from the vibrational ground level of the excited electronic state into a vibrational level of the electronic ground state. Again, also in these approaches only the projections of the cross-sections onto the focal plane were determined.

b) Beyond 2-level systems: vibronic excitation and incoherent vibrational relaxation

For some molecules (< 10%) we observed delay traces as shown in Fig. 4 (black line), that are similar to the curve in Fig. 2c, but feature a significantly longer rise time of several 100 fs and a higher contrast (ratio between the count rates at $\Delta t = 600$ fs and $\Delta t = 0$ fs). The relative phase between the pulses was fixed at $\phi = 0$ rad, and the excitation intensity was constant as before. These traces could not be reproduced by simulations based on a purely electronic 2-level system even for a physically unreasonable choice of fit parameters. We therefore extended the model to a 3-level system including incoherent vibrational relaxation in the electronically excited state (Fig. 4, inset): the central laser frequency is resonant with the transition between the electronic ground state and a vibrational level in the excited state ($|1\rangle \leftrightarrow |3\rangle$). The excitation relaxes incoherently into the vibrational ground level of the excited state (level $|2\rangle$) with a time constant τ_{vib} before radiative decay back into the ground state.

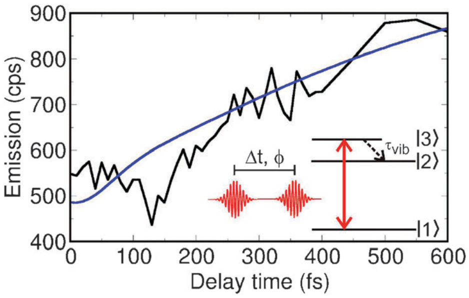

Fig. 4 Ultrafast double-pulse excitation of a 3-level system at room temperature. Black line: single-molecule fluorescence as a function of the delay time between the pulses ($\phi = 0$ rad, cps: counts per second). Blue line: numerical simulations based on the optical Bloch equations for a 3-level system yielding: $\omega_{R,0} = 0.05$ fs^{-1}, $\gamma_2{}^* = 0.008$ fs^{-1}, $\delta = 0$ cm^{-1}, $\mu_{12,\mathrm{eff}} = 7.9$ D, $\tau_{\mathrm{vib}} = 500$ fs. Inset: A 3-level system is resonantly excited into a vibrational level $|3\rangle$ of the electronically excited state. The excitation decays into the vibrational ground level of the excited state $|2\rangle$ with a time constant t_{vib} (vibrational relaxation) before radiative decay into the ground state $|1\rangle$.

The optical Bloch equations can be easily adapted to this 3-level system (see *e.g.* ref. 33). Following the approach described above, we computed the population probability in state $|2\rangle$ after interaction of the pulse sequence with the molecule to retrieve the fit parameters. For the data shown in Fig. 4 the best fit yields $\tau_{\mathrm{vib}} \sim 500$ fs ($\omega_{R,0} = 0.05$ fs^{-1}, $\gamma_2{}^* = 0.008$ fs^{-1}, $\delta = 0$ cm^{1}, $\mu_{12,\mathrm{eff}} = 7.9$ D; Fig. 4, blue line). For other molecules, that also show this type of delay traces, we found time constants τ_{vib} between 300 and 500 fs. Given the limited time window of 600 fs, however, these numbers should be considered as lower bounds only. Since the τ_{vib} values are in agreement with sub-picosecond intra-molecular vibrational relaxation (IVR) times recorded for bulk TDI in solution[21] and for other large organic molecules,[34] τ_{vib} is attributed accordingly to IVR.

The shape of the trace in Fig. 4 can be interpreted in a similar way as that in Fig. 2c: At short delay times stimulated absorption and emission processes are induced by the laser pulse(s) (Rabi-oscillations), as indicated by the rather high maximum Rabi-frequency ($\omega_{R,0} = 0.05$ fs^{-1}, Fig. 4). This results in a small excited state probability after interaction of the pulse sequence with the molecule. For increasing Δt the Rabi-oscillations are damped by dephasing processes and more population probability is left in the excited state. However, the underlying dephasing mechanism is now different as compared to the case displayed in Fig. 2c. Here, both pure dephasing processes and incoherent population relaxation from level $|3\rangle$ into the vibrational ground level of the electronically excited state $|2\rangle$ cause the damping of the Rabi-oscillations. Pure electronic dephasing affects the shape of the curve in Fig. 4 in the first *ca.* 100 fs, while IVR gives rise to the long rising behaviour with time constants of 300–500 fs.

The small number of molecules featuring delay traces as depicted in Fig. 4 is not surprising, since we have chosen the central excitation wavelength to be near-resonant with the purely electronic transition of the ensemble absorption spectrum. However, there is a small probability that a particular single molecule features a highly red-shifted absorption and its electronic transition is then in the lowest-energy tail of the bulk spectrum. Consequently, the excitation becomes (near-)-resonant with a vibronic transition in agreement with the 3-level model.

Several years ago, van Dijk *et al.*[13,14] employed a fluorescence-detected incoherent pump–probe scheme on single molecules using high-intensity saturating pulses. They observed rising emission signals as a function of the delay time between the pulses, similar to the traces shown in Fig. 2c and 4, and retrieved widely distributed rise times ranging from *ca.* 50 fs up to 1.3 ps. However, in those experiments the pulse width was rather long with 280 fs and the pulse sequences were not phase-controlled. Consequently, coherent effects were averaged out, and based on a rate equation model for a 3-level system the rising shape of the traces was attributed to incoherent IVR in the electronically excited state, in analogy to the incoherent mechanism described above. In the light of our results presented here, van Dijk's data should be reinterpreted: the rise times shorter than *ca.* 100–200 fs are probably due to purely electronic dephasing in a 2-level system, similar to our rising traces recorded at high Rabi-frequencies (high excitation intensities, Fig. 2c). Only the longer rise times of up to 1.3 ps, that were observed by van Dijk *et al.* on a few molecules,[13] very likely come from IVR in the excited electronic state.

c) Beyond 2-level systems: excited state vibrational wave-packets

In the approach described above the pulse width is rather long and thus only a single vibronic transition of an individual molecule is excited. Hence, information on vibrational modes in the excited state is limited to incoherent vibrational relaxation times and to the detuning from the (near-)resonant transition. Absolute values for the energies and coupling strengths of vibrational modes in the excited state can not be obtained, *i.e.* information on the shape and relative displacement of the potential energy surfaces in the ground and excited electronic states.

In order to determine such parameters we excited single DNQDI-molecules with broadband pulses (spectral band width 120 nm, pulse duration 15 fs), which overlap basically with the entire absorption spectrum of this molecule. Thus, a manifold of vibronic states is excited coherently and a coherent superposition of vibrational levels is created.[35,36] This excited state vibrational wave-packet is non-stationary and moves periodically across the potential energy surface with a period that is inversely proportional to the energies of the vibrational modes (Fig. 5a). Hence, measuring wave-packet oscillations directly reports on the properties of the excited state potential energy surface.

In our single-molecule experiment we visualise wave-packet oscillations by a double-pulse excitation scheme,[15] because control over the relative phase and delay between pulses leads to interference between consecutively excited wave-packets.[35] The first pulse excites a vibrational wave-packet that travels around the excited state potential surface (Fig. 5a). If both pulses are in-phase ($\phi = 0$ rad), the second pulse launches a

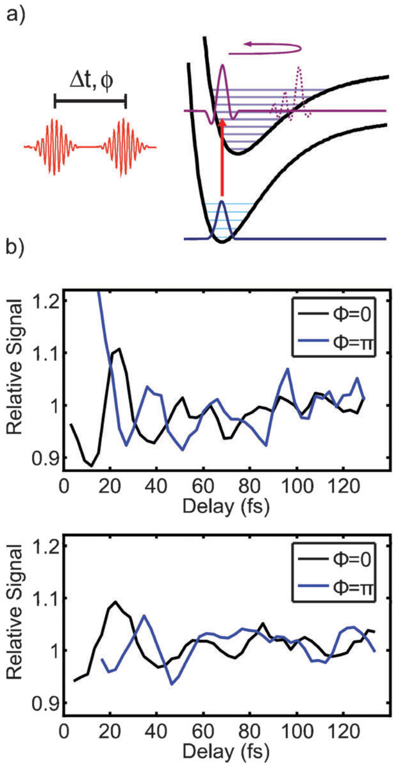

Fig. 5 Wave-packet interference in single molecules at room temperature. (a) A broadband double-pulse sequence excites a vibrational wave-packet that travels periodically in the excited state potential energy surface. This oscillatory behaviour is visualised by a phase-locked time-delayed pulse, which creates a second wave-packet and gives rise to wave-packet interference. (b) Fluorescence of two single molecules as a function of the delay time for in-phase (black) and out-of-phase pulses (blue), respectively.

wave-packet that has the same initial phase as the first one. When the wave-packets do not overlap in the Franck–Condon region of the potential energy surface and thus do not interact with each other, the population transfer is proportional to the intensity of both pulses. However, when both wave-packets are overlapping in the Frank-Condon region, the wave-packets will interfere constructively, thereby transferring more population probability to the excited state than given simply by the intensity of both pulses. Finally, when the wave-packets are prepared out-of-phase with each other by a π phase difference between the exciting pulses and overlap in the Franck–Condon region, destructive interference will dump population probability back to the ground state. In such two-pulse schemes the excited state population, *i.e.* the fluorescence signal, created after interaction with the double-pulses oscillates as a function of the delay.

In Fig. 5b the result of this experiment is shown for two single DNQDI-molecules; note the much shorter time axes with respect to the data shown in Fig. 2 and 4. The relative phase between the pulses is 0 (black curves) and π rad (blue curves), respectively. The excitation power was constant during acquisition of each trace and was kept significantly below saturation levels.[15] A clear oscillatory behaviour of the fluorescence is observed in all traces and interpreted accordingly as wave-packet interference. Vibrational energies were retrieved from these data by a Fourier transform that yielded a single dominant vibrational mode for each molecule. This analysis was performed on a total of 52 molecules and vibrational frequencies between 670 and 1500 cm^{-1} with a peak at 1070 cm^{-1} were found[15] that are in agreement with those reported for bulk DNQDI,[20] *e.g.* carbon-bond and C–N stretch modes. The spreading of vibrational frequencies is ascribed to a broad distribution of coupling strength of different vibrational modes to the electronic transitions and to distributions of the vibrational energies. This is caused by conformational constraints imposed by the surrounding polymer matrix as well as by locally varying electrostatic interactions between DNQDI-molecules and the host.[24,37]

The decay in the oscillations results from dephasing processes that lead to a loss of phase memory between the vibrational modes constituting the wave-packet. The corresponding time constants are about 50 fs and agree with those measured for the coherence decay on TDI (Fig. 2b, c and 3b). This indicates that the wave-packet decay likely results from pure dephasing due to interaction with the PMMA-matrix, and not from incoherent (intramolecular) vibrational relaxation.

Because the excitation and interference of wave-packets is a coherent process, it can be influenced by altering the phase between the pulses. More specifically, a phase difference of π should give an exactly inverted oscillatory trace. This is demonstrated by the blue curves in Fig. 5b for two molecules. As is readily observed the dominant frequencies and dephasing times are the same, but the oscillations of the traces are out of phase.

Conclusion

In conclusion, we presented results on femtosecond phase-controlled excitation of single molecules embedded in a disordered matrix at room temperature, and demonstrated the feasibility of this approach to gain insights into ultrafast intra-molecular processes as well as interactions with the local environments. These techniques will be extended to investigate ultrafast (in-)coherent excitation energy transfer dynamics in more complex multichromophoric systems, such as natural photosynthetic and artificial dendritic light-harvesting assemblies.

Acknowledgements

We thank T. H. Taminiau and F. Kulzer for discussions and assistance with the experimental setup, and K. Müllen for providing the molecules. We also appreciate technical assistance of Peter Fendel (Menlo Systems) with the Octavius laser system, and the collaboration with Biophotonics Solutions Inc. in developing the double-pass pulse shaper. Funding by the Körber foundation (Hamburg), the Spanish ministry of science and innovation (CSD2007-046-NanoLight.es and MAT2006-08184), the European Union (FP6 Bio-Light-Touch and ERC advanced investigators grant) is gratefully acknowledged.

References

1 W. E. Moerner and L. Kador, *Phys. Rev. Lett.*, 1989, **62**, 2535–2538; M. Orrit and J. Bernard, *Phys. Rev. Lett.*, 1990, **65**, 2716–2719.

2 C. Hofmann, T. J. Aartsma, H. Michel and J. Köhler, *Proc. Natl. Acad. Sci. U. S. A.*, 2003, **100**, 15534–15538; X. Michalet, S. Weiss and M. Jäger, *Chem. Rev.*, 2006, **106**, 1785–1813.

3 J. Elf, G. Li and X. S. Xie, *Science*, 2007, **316**, 1191–1194.

4 R. Zondervan, F. Kulzer, G. C. G. Berkhout and M. Orrit, *Proc. Natl. Acad. Sci. U. S. A.*, 2007, **104**, 12628–12633.

5 D. A. Vanden Bout, W. T. Yip, D. Hu, D. K. Fu, T. M. Swager and P. F. Barbara, *Science*, 1997, **277**, 1074–1077; F. Schindler, J. M. Lupton, J. Feldmann and U. Scherf, *Proc. Natl. Acad. Sci. U. S. A.*, 2004, **101**, 14695–14700; R. Hildner, U. Lemmer, U. Scherf, M. van Heel and J. Köhler, *Adv. Mater.*, 2007, **19**, 1978–1982; H. Lin, S. R. Tabaei, D. Thomsson, O. Mirzov, P. O. Larsson and I. G. Scheblykin, *J. Am. Chem. Soc.*, 2008, **130**, 7042–7051; F. C. de Schryver, T. Vosch, M. Cotlet, M. van der Auweraer, K. Müllen and J. Hofkens, *Acc. Chem. Res.*, 2005, **38**, 514–522; R. Métivier, F. Kulzer, T. Weil, K. Müllen and T. Basché, *J. Am. Chem. Soc.*, 2004, **126**, 14364–14365.

6 A. M. van Oijen, M. Ketelaars, J. Köhler, T. J. Aartsma and J. Schmidt, *Science*, 1999, **285**, 400–402; M. A. Bopp, A. Sytnik, T. D. Howard, R. J. Cogdell and R. M. Hochstrasser, *Proc. Natl. Acad. Sci. U. S. A.*, 1999, **96**, 11271–11276; S. Mackowski, S. Wörmke, T. H. P. Brotosudarmo, H. Scheer and C. Bräuchle, *Photosynth. Res.*, 2007, **95**, 253–260.

7 J. P. Hoogenboom, G. Sanchez-Mosteiro, G. Colas des Francs, D. Heinis, G. Legay, A. Dereux and N. F. van Hulst, *Nano Lett.*, 2009, **9**, 1189–1195.

8 J. Hwang, M. Pototschnig, R. Lettow, G. Zumofen, S. Götzinger and V. Sandoghdar, *Nature*, 2009, **460**, 76–80.

9 R. van Grondelle and V. I. Novoderezhkin, *Phys. Chem. Chem. Phys.*, 2006, **8**, 793–807; I. G. Scheblykin, A. Yartsev, T. Pullerits, V. Gulbinas and V. Sundström, *J. Phys. Chem. B*, 2007, **111**, 6303–6321.

10 G. Panitchayangkoon, D. Hayes, K. A. Fransted, J. R. Caram, E. Harel, J. Wen, R. E. Blankenship and G. S. Engel, *Proc. Natl. Acad. Sci. USA*, 2010, **107**, 12766–12770; E. Collini, C. W. Wong, K. E. Wilk, P. M. G. Curmi, P. Brumer and G. D. Scholes, *Nature*, 2010, **463**, 644–647.

11 E. Collini and G. D. Scholes, *Science*, 2009, **323**, 369–373.

12 D. G. Kuroda, C. P. Singh, Z. Peng and V. D. Kleiman, *Science*, 2009, **326**, 263–267.

13 E. M. H. P. van Dijk, J. Hernando, J. García-López, M. Crego-Calama, D. N. Reinhoudt, L. Kuipers, M. F. García-Parajó and N. F. van Hulst, *Phys. Rev. Lett.*, 2005, **94**, 078302; E. M. H. P. van Dijk, J. Hernando, M. F. García-Parajó and N. F. van Hulst, *J. Chem. Phys.*, 2005, **123**, 064703.

14 J. Hernando, E. M. H. P. van Dijk, J. P. Hoogenboom, J. García-López, D. N. Reinhoudt, M. Crego-Calama, M. F. García-Parajó and N. F. van Hulst, *Phys. Rev. Lett.*, 2006, **97**, 216403.

15 D. Brinks, F. D. Stefani, F. Kulzer, R. Hildner, T. H. Taminiau, Y. Avlasevich, K. Müllen and N. F. van Hulst, *Nature*, 2010, **465**, 905–908.

16 R. Hildner, D. Brinks and N. F. van Hulst, *Nature Phys.*, 2010, DOI: 10.1038/nphys1858.

17 O. E. Martínez, *IEEE J. Quantum Electron.*, 1987, **23**, 1385–1387.

18 D. Brinks, F. D. Stefani and N. F. van Hulst, in *Ultrafast Phenomena XVI*, ed. P. Corkum, S. de Silvestri, K. A. Nelson, E. Riedle and R. W. Schoenlein, Springer, Berlin, Heidelberg, 2009, pp. 890–892.

19 S. Mais, J. Tittel, T. Basché, C. Bräuchle, W. Göhde, H. Fuchs, G. Müller and K. Müllen, *J. Phys. Chem. A*, 1997, **101**, 8435–8440; F. O. Holtrup, G. R. J. Müller, H. Quante, S. De Feyter, F. C. De Schryver and K. Müllen, *Chem.–Eur. J.*, 1997, **3**, 219–225.

20 Y. Avlasevich, S. Müller, P. Erk and K. Müllen, *Chem.–Eur. J.*, 2007, **13**, 6555–6561.

21 G. Schweitzer, R. Gronheid, S. Jordens, M. Lor, G. De Belder, T. Weil, E. Reuther, K. Müllen and F. C. De Schryver, *J. Phys. Chem. A*, 2003, **107**, 3199–3207.

22 A. H. Zewail, *Acc. Chem. Res.*, 1980, **13**, 360–368.

23 L. Allen and J. H. Eberly, *Optical Resonance and Two-Level Atoms*, Dover, New York, 1987; R. Loudon, *The Quantum Theory of Light*, Oxford University Press, Oxford, New York, 2000.

24 J. J. Macklin, J. K. Trautman, T. D. Harris and L. E. Brus, *Science*, 1996, **272**, 255–258.

25 G. Hinze, R. Metivier, F. Nolde, K. Müllen and T. Basché, *J. Chem. Phys.*, 2008, **128**, 124516.

26 C. J. Bardeen, G. Cerullo and C. V. Shank, *Chem. Phys. Lett.*, 1997, **280**, 127–133; Y. Nagasawa, S. A. Passino, T. Joo and G. R. Fleming, *J. Chem. Phys.*, 1997, **106**, 4840–4852.

27 M. Orrit, J. Bernard and R. I. Personov, *J. Phys. Chem.*, 1993, **97**, 10256–10268.

28 B. Fückel, A. Köhn, M. E. Harding, G. Diezemann, G. Hinze, T. Basché and J. Gauss, *J. Chem.Phys.*, 2008, **128**, 074505.

29 D. Patra, I. Gregor and J. Enderlein, *J. Phys. Chem. A*, 2004, **108**, 6836–6841.

30 M. Celebrano, P. Kukura, A. Renn and V. Sandoghdar, *Nat. Photon.*, advance online publication, 9 January 2011, DOI: 10.1038/nphoton.2010.290.

31 A. Gaiduk, M. Yorulmaz, P. V. Ruijgrok and M. Orrit, *Science*, 2010, **330**, 353–356.

32 L. Kastrup and S. W. Hell, *Angew. Chem., Int. Ed.*, 2004, **43**, 6646–6649.

33 R. Brown, J. Wrachtrup, M. Orrit, J. Bernard and C. von Borczyskowski, *J. Chem. Phys.*, 1994, **100**, 7182–7191.

34 M. J. Rosker, F. W. Wise and C. L. Tang, *Phys. Rev. Lett.*, 1986, **57**, 321–324; J. Liu, W. Fan, K. Han, W. Deng, D. Xu and N. Lou, *J. Phys. Chem. A*, 2003, **107**, 10857–10861; A. Weigel and N. P. Ernsting, *J. Phys. Chem. B*, 2010, **114**, 7879–7893.

35 N. F. Scherer, R. J. Carlson, A. Matro, M. Du, A. J. Ruggiero, V. Romero-Rochin, J. A. Cina, G. R. Fleming and S. A. Rice, *J. Chem. Phys.*, 1991, **95**, 1487–1511.

36 K. Ohmori, *Annu. Rev. Phys. Chem.*, 2009, **60**, 487–511.

37 I. Renge, *J. Opt. Soc. Am. B*, 1992, **9**, 719–723; A. B. Myers, P. Tchénio, M. Z. Zgierski and W. E. Moerner, *J. Phys. Chem.*, 1994, **98**, 10377–10390.